

Quadrupole association and dissociation of hydrogen in the early universe

Robert C Forrey[†]

Department of Physics, Pennsylvania State University, Berks Campus, Reading, PA 19610-6009, USA

Abstract. Radiative association and photodissociation rates are calculated for quadrupole transitions of H_2 . A complete set of bound and unbound states are included in a self-consistent master equation to obtain steady-state concentrations for a dilute system of hydrogen atoms and molecules. Phenomenological rate constants computed from the steady-state concentrations satisfy detailed balance for any combination of matter and radiation temperature. Simple formulas are derived for expressing the steady-state distributions in terms of equilibrium distributions. The rate constant for radiative association is found to be generally small for all temperature combinations. The photodissociation rate constant for quadrupole transitions is found to dominate the rate constants for other H_2 photodestruction mechanisms for $T_R \leq 3000$ K. Implications for the formation and destruction of H_2 in the early universe are discussed.

[†] E-mail:rcf6@psu.edu

1. Introduction

It is widely accepted that hydrogen molecules catalyzed the formation of the first stars in the universe [1–5]. As primordial condensations formed, the gas density increased and subsequent collisions produced internally excited states which quenched via the emission of electric quadrupole radiation. Although inefficient, the removal of the quadrupole radiation from the condensation allowed gravitational collapse to proceed toward the eventual first star. The probability of a quadrupole transition scales as the fifth power of the difference in internal energy levels [6, 7]. Therefore, unbound and quasibound states which provide large energy differences might play a role in the early stages of cooling. Nevertheless, the possibility that hydrogen atoms could form molecules via the emission of quadrupole radiation has so far been neglected. Considering that the main processes leading to the formation of H_2 are known to be quite slow, it is worth investigating the quadrupole association mechanism to see whether it makes a significant contribution to the formation rate. Such a study is particularly compelling in light of recent developments [8] concerning the role of quasibound states in the recombination process. It was shown for conditions of local thermodynamic equilibrium (LTE) that long-lived orbiting resonances can enhance the radiative association (RA) rate constant by several orders of magnitude [9] compared to calculations where they are neglected. Hydrogen interactions allow orbiting resonances whose lifetimes are extremely long (some are comparable to the age of the universe [10]). Such resonances can provide feedback which may further enhance the formation rates when the gas is not in LTE as is the case in the early universe after the matter and radiation temperatures have decoupled. Therefore, in the present work, we provide a complete account of all resonant and non-resonant contributions for the RA process



where ν represents the photon released in a quadrupole transition.

The inverse process of photodissociation via quadrupole transitions is also considered. Photodissociation of H_2 is believed to be important in the early universe. Direct collapse to a supermassive black hole may occur if there are no hydrogen molecules to promote cooling and fragmentation [11]. A strong radiation field, such as may occur after ignition of the first stars, destroys the formation of H^- and H_2^+ which are precursors for the formation of H_2 . Direct and indirect photodissociation via dipole transitions to the Lyman and Werner states deplete H_2 at high energies. The critical value of the Lyman and Werner intensity J_{21}^{crit} needed for supermassive star formation [12, 13] is determined by the relative strength of the rate constants for photodestruction of H^- , H_2^+ , and H_2 . Because quadrupole radiation allows transitions within the same ground electronic state, the mechanism would apply at both low and high radiation temperatures and perhaps contribute to the depletion of H_2 .

In order to perform the study, we use the self-consistent quantum kinetic theory developed previously [8] which computes the rate constants from the steady-state solution of a Sturmian master equation. The bound and unbound energy eigenstates of the Sturmian representation form a complete basis set for both the dynamics and kinetics. Consequently, all transitions between bound and unbound states, which include long-lived quasibound and discretized non-resonant states, are accounted for. The summed rate coefficients are then used to provide phenomenological rate constants for an idealized system consisting of dilute hydrogen atoms and molecules which undergo negligible inelastic collisions. The RA and photodissociation rate constants computed in this way are guaranteed to satisfy detailed balance for any combination of matter and radiation temperature. Therefore, these rate constants are suitable for use in an expanded network of chemical processes. In the present work, however, we consider only the quadrupole mechanism for association and dissociation of hydrogen and draw conclusions about its importance in the early universe.

2. Theory

We begin by considering the rate equation

$$\frac{d}{dt}[H_2] = M_r[H]^2 - M_d[H_2] \quad (2)$$

for a fixed number density of hydrogen nuclei

$$n_H = [H] + 2[H_2] \quad (3)$$

where square brackets indicate the concentration of the enclosed species, and M_r and M_d are the respective rate constants for recombination and dissociation. The solution to the rate equation may be written

$$[H_2] = \frac{\left(\frac{n_H}{2}\right)^2 (1 - e^{-\lambda t})}{\alpha + \beta + (\alpha - \beta)e^{-\lambda t}} \quad (4)$$

$$\alpha = \frac{\lambda}{8M_r} \quad (5)$$

$$\beta = \frac{4M_r n_H + M_d}{8M_r} \quad (6)$$

$$\lambda = (8M_r M_d n_H + M_d^2)^{1/2}. \quad (7)$$

The rate constants in equation (2) are calculated using the quantum kinetic theory described previously [8]. This method requires that the single rate equation (2) be consistent with a Sturmian master equation which contains all possible transitions, including those involving the discretized continuum. In general, the state-to-state transition probability is given by

$$M_{i \rightarrow j} = \begin{cases} A_{i \rightarrow j} + B_{i \rightarrow j} \bar{J}_{i \rightarrow j} + C_{i \rightarrow j} & E_i > E_j \\ B_{i \rightarrow j} \bar{J}_{i \rightarrow j} + C_{i \rightarrow j} & E_j > E_i \end{cases} \quad (8)$$

where A and B are Einstein coefficients, C is a collisional rate coefficient, and \bar{J} is the average radiation field at the frequency corresponding to a molecular transition between states with energies E_i and E_j . The master equation may be divided into two sets of equations corresponding to bound (b) and unbound (u) states

$$\begin{aligned} \frac{d}{dt}[H_2(b_i)] &= \sum_j (M_{u_j \rightarrow b_i}[H_2(u_j)] - M_{b_i \rightarrow u_j}[H_2(b_i)]) \\ &+ \sum_{j \neq i} (M_{b_j \rightarrow b_i}[H_2(b_j)] - M_{b_i \rightarrow b_j}[H_2(b_i)]) \end{aligned} \quad (9)$$

$$\begin{aligned} \frac{d}{dt}[H_2(u_i)] &= \sum_j (M_{b_j \rightarrow u_i}[H_2(b_j)] - M_{u_i \rightarrow b_j}[H_2(u_i)]) \\ &+ \sum_{j \neq i} (M_{u_j \rightarrow u_i}[H_2(u_j)] - M_{u_i \rightarrow u_j}[H_2(u_i)]) \\ &+ k_{f \rightarrow u_i}^{elastic}[H]^2 - \tau_{u_i}^{-1}[H_2(u_i)] \end{aligned} \quad (10)$$

where τ_{u_i} is the lifetime of the unbound state u_i , and $k_{f \rightarrow u_i}^{elastic}$ is the two-body elastic scattering rate constant for a discretized free (f) state, which is related to $\tau_{u_i}^{-1}$ by the equilibrium constant

$$K_{u_i}^{eq} = \frac{g_{u_i} \exp(-E_{u_i}/k_B T)}{Q_H^2 Q_T}. \quad (11)$$

$Q_H = 4$ is the atomic partition function[‡], $g_u = (2I_u + 1)(2j_u + 1)$ is the degeneracy of the unbound state ($I_u = 0$ for para- H_2 and $I_u = 1$ for ortho- H_2), Q_T is the translational partition function for temperature T , and k_B is Boltzmann's constant.

[‡] For the temperatures considered in the present work, the H atom is assumed to be in the ground state, and the atomic partition function is due to electron and nuclear spin degeneracy.

The steady-state solution to the master equation yields the rate constants

$$M_r = \frac{\sum_{ij} g_{u_i} e^{-E_{u_i}/k_B T} (1 + \delta_{u_i}) M_{u_i \rightarrow b_j}^{\text{OUT}}}{Q_H^2 Q_T} \quad (12)$$

and

$$M_d = \frac{\sum_{ij} g_{b_i} e^{-E_{b_i}/k_B T} (1 + \delta_{b_i}) M_{b_i \rightarrow u_j}^{\text{OUT}}}{Q_{H_2}} \quad (13)$$

where

$$Q_{H_2} = \sum_i (1 + \delta_{b_i}) g_{b_i} \exp(-E_{b_i}/k_B T) \quad (14)$$

is the molecular partition function, δ_b and δ_u are non-LTE concentration defects which may be obtained from the steady-state concentrations

$$1 + \delta_{b_i} = \frac{\left(\frac{Q_{H_2}[H_2(b_i)]}{[H_2]} \right)_{\text{SS}}}{\left(\frac{Q_{H_2}[H_2(b_i)]}{[H_2]} \right)_{\text{LTE}}} = \sum_{j,k,l} \tilde{A}_{b_i b_j}^{-1} M_{b_j \rightarrow u_k}^{\text{IN}} \tilde{B}_{u_k u_l}^{-1} \quad (15)$$

$$1 + \delta_{u_i} = \frac{\left(\frac{[H_2(u_i)]}{[H]^2} \right)_{\text{SS}}}{\left(\frac{[H_2(u_i)]}{[H]^2} \right)_{\text{LTE}}} = \sum_j \tilde{B}_{u_i u_j}^{-1} \quad (16)$$

and the matrices \tilde{A} and \tilde{B} and the rate coefficients $M_{i \rightarrow j}^{\text{IN}}$ and $M_{i \rightarrow j}^{\text{OUT}}$ are defined below. Equations (15) and (16) give the identity

$$1 = \frac{\sum_{ij} g_{u_i} e^{-E_{u_i}/k_B T} (1 + \delta_{u_i}) M_{u_i \rightarrow b_j}^{\text{OUT}}}{\sum_{ij} g_{b_i} e^{-E_{b_i}/k_B T} (1 + \delta_{b_i}) M_{b_i \rightarrow u_j}^{\text{OUT}}} \quad (17)$$

so that the ratio

$$\frac{M_r}{M_d} = \frac{[H_2]}{[H]^2} = \frac{Q_{H_2}}{Q_H^2 Q_T} \quad (18)$$

reduces to the statistical Saha relation when all $\delta_b = \delta_u = 0$. The matrices \tilde{A} and \tilde{B} which need to be inverted are obtained from equations (9) and (10) and are given by

$$\tilde{A}_{b_i b_j} = \delta_{ij} \left(\sum_{k \neq i} M_{b_i \rightarrow b_k}^{\text{OUT}} + \sum_k M_{b_i \rightarrow u_k}^{\text{OUT}} \right) - (1 - \delta_{ij}) M_{b_i \rightarrow b_j}^{\text{IN}} \quad (19)$$

$$\begin{aligned} \tilde{B}_{u_i u_j} = \delta_{ij} \left\{ 1 + \tau_{u_i} \left(\sum_{k \neq i} M_{u_i \rightarrow u_k}^{\text{OUT}} + \sum_k M_{u_i \rightarrow b_k}^{\text{OUT}} \right) \right\} \\ - \tau_{u_i} \left\{ (1 - \delta_{ij}) M_{u_i \rightarrow u_j}^{\text{IN}} + \sum_{k,l} M_{u_i \rightarrow b_k}^{\text{IN}} \tilde{A}_{b_k b_l}^{-1} M_{b_l \rightarrow u_j}^{\text{IN}} \right\}. \end{aligned} \quad (20)$$

In the present work, we exclude inelastic collisions so that $C_{i \rightarrow j} \equiv 0$ in equation (8). Assuming a complete redistribution of frequencies [14], the average radiation field may be written in terms of the Planck black-body radiation function, $P_{i \rightarrow j}$, and a line source function, $S_{i \rightarrow j}$, as follows [15]

$$\bar{\mathcal{J}}_{i \rightarrow j}(T_M, T_R) = (1 - \beta_{ij}) S_{i \rightarrow j}(T_M) + \beta_{ij} P_{i \rightarrow j}(T_R) \quad (21)$$

where β_{ij} is the escape probability for a photon associated with the $i \rightarrow j$ transition, and the dependence of the matrix elements on matter temperature T_M and radiation temperature T_R is now shown. The line source function may be written

$$S_{i \rightarrow j}(T_M) = F(\nu_{ij}) \left(\frac{g_i n_j}{g_j n_i} - 1 \right)^{-1} \quad (22)$$

where n_i and n_j are level densities, ν_{ij} is the frequency of the line photon, and $F(\nu)$ is the usual Planck function coefficient. Because the source function (22) is derived for conditions of statistical equilibrium, it does not contribute to the matrix elements in the steady-state equations (19) and (20). These matrices are then obtained from the Planck function and the Maxwell-Boltzmann factor arising from elastic collisions and may be written as

$$M_{i \rightarrow j}^{\text{IN}}(T_M, T_R) = \frac{g_j}{g_i} e^{-(E_j - E_i)/k_B T_M} M_{j \rightarrow i}^{\text{OUT}}(T_R) \quad (23)$$

and

$$M_{i \rightarrow j}^{\text{OUT}}(T_R) = \beta_{ij} R_{i \rightarrow j}(T_R) \quad (24)$$

with

$$R_{i \rightarrow j}(T_R) = \frac{A_{i \rightarrow j}}{1 - e^{-(E_i - E_j)/k_B T_R}}. \quad (25)$$

There is no T_M -dependence in the outgoing rate coefficient (24) due to the assumption that inelastic collisions are negligible. In order to determine δ_{b_i} and δ_{u_i} , it is necessary to compute \tilde{A} and \tilde{B} . In practical computations, equations (19) and (20) tend to suffer round-off errors, particularly at low temperatures where the probability for upward transitions can be very small. For such conditions, the inversion of \tilde{A} may be handled analytically

$$y_{b_i u_j} = \sum_k \tilde{A}_{b_i b_k}^{-1} M_{b_k \rightarrow u_j}^{\text{IN}} \quad (26)$$

$$\approx \frac{e^{-E_{b_i}(1/k_B T_R - 1/k_B T_M)} \sum_k g_{b_k} e^{-E_{b_k}/k_B T_M} M_{b_k \rightarrow u_j}^{\text{IN}}}{\sum_{kl} g_{b_k} e^{-E_{b_k}/k_B T_R} M_{b_k \rightarrow u_l}^{\text{OUT}} \delta_{I_i I_k}}. \quad (27)$$

The δ -function in the denominator arises from the impossibility of an ortho-para transition for quadrupole radiation. If three-body collisions were included in $M_{i \rightarrow j}$, equation (27) would need to be modified to include inelastic and exchange reactions. This problem was considered previously [8] where it was shown that all of the unbound states reach a steady-state concentration that is well-approximated by a Boltzmann distribution whenever three-body collisions are important. In the present work, the approximate formula (27) is expected to be reliable when $M_{b \rightarrow u}^{\text{OUT}}$ is less than $M_{b \rightarrow b'}^{\text{OUT}}$. This condition, which is nearly always met, yields the result

$$1 + \delta_{b_i} = C_{I_i} e^{-E_{b_i}(1/k_B T_R - 1/k_B T_M)} \quad (28)$$

where

$$C_{I_i} = \frac{\sum_{jk} g_{u_j} e^{-E_{u_j}/k_B T_M} (1 + \delta_{u_j}) M_{u_j \rightarrow b_k}^{\text{OUT}} \delta_{I_i I_j}}{\sum_{jk} g_{u_j} e^{-E_{u_j}/k_B T_R} M_{u_j \rightarrow b_k}^{\text{OUT}} \delta_{I_i I_j}} \quad (29)$$

is a symmetry constant for para-H₂ and ortho-H₂ which depends only on T_M and T_R . This allows equation (13) to be written

$$M_d = \frac{\sum_{ij} C_{I_i} g_{b_i} e^{-E_{b_i}/k_B T_R} M_{b_i \rightarrow u_j}^{\text{OUT}}}{\sum_i C_{I_i} g_{b_i} e^{-E_{b_i}/k_B T_R}}. \quad (30)$$

All of the T_M -dependence in the photodissociation rate constant (30) is contained in the symmetry constant. If C_I is approximately the same for both nuclear symmetries, then it is a good approximation to use a Boltzmann distribution of states for $T = T_R$. The δ_{u_i} may be obtained by substituting equation (27) into equation (20) to yield

$$\begin{aligned} \tilde{B}_{u_i u_j} = & \delta_{ij} \left\{ 1 + \tau_{u_i} \left(\sum_{k \neq i} M_{u_i \rightarrow u_k}^{\text{OUT}} + (1 - \epsilon_i) \sum_k M_{u_i \rightarrow b_k}^{\text{OUT}} \right) \right\} \\ & - (1 - \delta_{ij}) \tau_{u_i} \left(M_{u_j \rightarrow u_i}^{\text{OUT}} + \epsilon_i \sum_k M_{u_j \rightarrow b_k}^{\text{OUT}} \right) \\ & \times \frac{g_{u_j}}{g_{u_i}} e^{-(E_{u_j} - E_{u_i})/k_B T_M} \end{aligned} \quad (31)$$

where

$$\epsilon_i = \frac{g_{u_i} e^{-E_{u_i}/k_B T_R} \sum_k M_{u_i \rightarrow b_k}^{\text{OUT}}}{\sum_j g_{u_j} e^{-E_{u_j}/k_B T_R} \sum_k M_{u_j \rightarrow b_k}^{\text{OUT}} \delta_{I_i I_j}}. \quad (32)$$

Equations (16), (31), and (32) may be used to express the system of equations for the non-LTE defects in the form

$$1 + \delta_{u_i} = \frac{1 + \tau_{u_i} \Psi_i^{\text{IN}}}{1 + \tau_{u_i} \Psi_i^{\text{OUT}}} \quad (33)$$

where

$$\begin{aligned} \Psi_i^{\text{IN}} = & \sum_{j \neq i} (1 + \delta_{u_j}) \frac{g_{u_j}}{g_{u_i}} e^{-(E_{u_j} - E_{u_i})/k_B T_M} \\ & \times \left(M_{u_j \rightarrow u_i}^{\text{OUT}} + \epsilon_i \sum_k M_{u_j \rightarrow b_k}^{\text{OUT}} \right) \end{aligned} \quad (34)$$

and

$$\Psi_i^{\text{OUT}} = \sum_{k \neq i} M_{u_i \rightarrow u_k}^{\text{OUT}} + (1 - \epsilon_i) \sum_k M_{u_i \rightarrow b_k}^{\text{OUT}}. \quad (35)$$

In the limiting case $T_R \rightarrow 0$, equation (32) yields $\epsilon_1 = 1$ for the lowest energy unbound state u_1 and $\epsilon_i = 0$ for all states with energy $E_{u_i} > E_{u_1}$. If ϵ_i is set to zero for all i , then the above formulas reduce to ones given previously [8]

$$\Psi_i^{\text{IN}} = \sum_{j > i} (1 + \delta_{u_j}) \frac{g_{u_j}}{g_{u_i}} e^{-(E_{u_j} - E_{u_i})/k_B T_M} A_{u_j \rightarrow u_i} \quad (36)$$

and

$$\Psi_i^{\text{OUT}} = \sum_{j < i} A_{u_i \rightarrow u_j} + \sum_j A_{u_i \rightarrow b_j} \quad (37)$$

which may be solved iteratively starting with the highest energy quasibound state and assuming that $\delta_{u_j} = 0$ for all unbound states that are not quasibound. If $\delta_{u_j} = -1$ for all unbound states with $j > i$, then the formula

$$1 + \delta_{u_i} = \frac{1}{1 + \tau_{u_i} \left(\sum_{j < i} A_{u_i \rightarrow u_j} + \sum_j A_{u_i \rightarrow b_j} \right)} \quad (38)$$

is obtained which may be substituted into equation (12) to yield the commonly-used Bain and Bardsley formula [16] for resonant radiative association.

3. Results

The bound and unbound states of H_2 were obtained by solving the radial Schrödinger equation

$$\left[\frac{1}{2\mu} \frac{d^2}{dr^2} - \frac{j(j+1)}{2\mu r^2} - v(r) + E_{vj} \right] \chi_{vj}(r) = 0, \quad (39)$$

where μ is the reduced mass and $v(r)$ is the H_2 potential of Schwenke [10]. The notation b and u is understood to mean a unit-normalized bound or unbound energy eigenstate characterized by the pair of quantum numbers (v, j) where v and j are the vibrational and rotational quantum numbers for the eigenstate χ_{vj} . These eigenstates were obtained by diagonalization in an orthonormal L^2 Sturmian basis set consisting of Laguerre polynomial functions as described previously [17]. The vibrational quantum number for an unbound eigenstate corresponds to the quadrature index and only has meaning with respect to the scale factor and number of basis functions.

The Einstein A-coefficient for a radiative transition between an initial state i and a final state f is given by [6, 7]

$$A_{i \rightarrow f} = 1.4258 \times 10^4 (E_i - E_f)^5 |\langle \chi_i | Q(R) | \chi_f \rangle|^2 f(j_i, j_f) \text{ s}^{-1} \quad (40)$$

where R is the internuclear distance, $Q(R)$ is the quadrupole moment, χ_i and χ_f are the energy eigenfunctions of the initial and final states, and the branching ratio is given by

$$f(j_i, j_f) = \begin{cases} \frac{3(j_i+1)(j_i+2)}{2(2j_i+1)(2j_i+3)} & j_f = j_i + 2 \\ \frac{j_i(j_i+1)}{(2j_i-1)(2j_i+3)} & j_f = j_i \\ \frac{3j_i(j_i-1)}{2(2j_i-1)(2j_i+1)} & j_f = j_i - 2 \end{cases} \quad (41)$$

The Sturmian representation was tested by computing the A-coefficients for all bound to bound transitions using the quadrupole moment provided by Wolniewicz et al. [7] Excellent agreement was found for all of the tabulated transitions.

Equation (40) also applies to transitions involving resonant and non-resonant unbound states. Tables 1-4 provide an extension of the published tables [7] to include transitions between bound and quasibound states. Only narrow quasibound states that are well-represented by a single Sturmian eigenstate are included in the tables. Figure 1 shows the cumulative radiative width

$$\Gamma_u = \sum_b A_{u \rightarrow b} \quad (42)$$

for para-H₂ and ortho-H₂ formation. The sharp resonances due to long-lived quasibound states are clearly evident. In virtually all previous work on RA, extremely narrow resonances of this kind have been neglected, either because they are difficult to resolve using a grid-based method or because of an assumed breakdown of perturbation theory [18–20]. Recently, it was shown [9] that such resonances increased the LTE rate constant for SiO formation by ~ 100 times compared to calculations where the resonances were neglected. A similar observation [8] was made for the RA rate constant for CH⁺ where it was also predicted that the non-LTE defects could contribute to a further increase (or decrease) compared to the LTE values.

To explore this possibility for H₂, we computed $M_{i \rightarrow j}^{\text{IN}}$ and $M_{i \rightarrow j}^{\text{OUT}}$ in order to evaluate the non-LTE defects. We assume $\beta_{ij} = 1$ which means there is no distortion of the background blackbody radiation field. This assumption is convenient but not necessary - the formulation works as written for an optically thick gas so long as the complete redistribution of frequencies [14] is assumed and the escape probabilities are calculated using the line source function (22). Figures 2-5 show the non-LTE defects for the four longest-lived quasibound states of hydrogen. The tunneling widths [10] for these states are 1.1×10^{-21} , 8.2×10^{-25} , 1.5×10^{-18} , and $6.0 \times 10^{-34} \text{ cm}^{-1}$ for $j=24, 29, 31$, and 32 , respectively. The curves were computed using the approximate formula (31) and compared with the exact equation (20) for a range of temperatures where the inversion of equation (19) was numerically stable. Excellent agreement was found in all of the comparisons. As expected, the plots show $\delta_u = 0$ in the LTE limit $T_R = T_M$. Complete removal of long-lived quasibound states corresponds to $\delta_u = -1$. The top panels of Figures 2-5 show that this condition is approached for low values of T_R when $T_M > T_R$. The depletion is greatest for the quasibound state with the smallest tunneling width ($j = 32$). For the largest tunneling width shown ($j = 31$), the depletion is not as complete - the steady-state population is about 8% of its LTE value (see Figure 4). For the majority of quasibound states that are not shown, the steady-state and LTE populations are nearly identical ($\delta_u \approx 0$) for all temperatures.

The middle and lower panels of Figures 2-5 show that $\delta_u > 0$ for intermediate and large values of T_R when $T_M \gg T_R$. For para-H₂, the curves increase with T_R

before reaching their largest values at $T_R \approx 200\text{--}300$ K where they begin to decrease. For ortho- H_2 , the pattern is similar, however, the curves reach their largest values at $T_R \approx 500$ K. The lower panels for both para- H_2 and ortho- H_2 show the curves uniformly decreasing for $T_R \geq 1000$ K. Interestingly, Figures 2-5 show that $\delta_u \gg 0$ when $T_M \ll T_R$ which shows that the steady-state density of quasibound states is much greater than the LTE density. This suggests that there may be a significant enhancement in the formation rate constant when $T_M < T_R$.

In order to see the effect of the steady-state populations, we plot the LTE and non-LTE rate constants in Figure 6. The top panel shows the para- H_2 and ortho- H_2 contributions to the LTE rate constant. The large hump centered around 1 K is due to a low energy $j = 4$ resonance which has a tunneling lifetime of $8.4 \times 10^{-6} \text{ cm}^{-1}$ [10]. Ortho- H_2 formation begins to dominate at temperatures above 100 K. The total LTE rate constant shows a broad maximum of $\sim 10^{-28} \text{ cm}^3 \text{ s}^{-1}$ near 500 K. The middle and lower panels of Figure 6 show how the non-LTE populations affect the rate constant for various T_R . For para- H_2 , the steady-state and LTE contributions are the same for $T_M < 50$ K when $T_R = 10$ K. As T_M is increased beyond 50 K, the curve for $T_R = 10$ K drops below the LTE curve. Results for lower values of T_R were found to be essentially the same as the $T_R = 10$ K curve and are not shown. For ortho- H_2 , the steady-state and LTE contributions are very nearly the same when T_M and T_R are both less than 100 K. This is due to the somewhat larger energies for the ortho- H_2 quasibound states compared to the $j = 4$ resonance. As T_R increases, the rate constants for both nuclear symmetries increase due to stimulated emission. The non-LTE rate constants may be larger or smaller than their LTE values due the behavior of δ_u shown in Figures 2-5.

The full set of δ_u may be used to compute the symmetry constants C_I defined by equation (29). These constants allow convenient computation of the non-LTE concentration defects δ_b from equation (28) and the photodissociation rate constant from equation (30). Numerical results confirmed that C_I is indeed a constant for all combinations of vibrational and rotational states of a given symmetry. The top panel of Figure 7 shows C_I as a function of T_M for $T_R = 1000, 2000, 5000$, and 10000 K using solid lines for $I = 0$ and dashed lines for $I = 1$. A significant T_M -dependence may be seen for these constants, however, there is only a weak dependence on the symmetry I , particularly at high temperatures. Therefore, the C_I in equation (30) approximately drops out which eliminates the T_M -dependence of the dissociation rate constant M_d . This weak T_M -dependence is again due to the assumption that inelastic collisions are negligible which causes the general rate constant M_d defined by equation (13) to be equal to the photodissociation rate constant (30). In this limit, the steady-state distribution of bound states at temperature T_M is well-approximated by a Boltzmann equilibrium distribution at temperature T_R .

While a Boltzmann distribution of molecular states at temperature T_R is a good approximation when inelastic collisions are negligible, it should be noted that there is a scale change associated with the partition functions

$$\Lambda(T_R, T_M) \equiv \frac{Q_{\text{H}_2}^{SS}}{Q_{\text{H}_2}^{LTE}} \quad (43)$$

which yields

$$\left(\frac{M_r}{M_d} \right)_{SS} = \Lambda(T_R, T_M) \left(\frac{M_r}{M_d} \right)_{LTE}. \quad (44)$$

The bottom panel of Figure 7 shows the scale factor for the quadrupole mechanism as a function of temperature. As expected, the figure shows $\Lambda = 1$ when $T_R = T_M$. However, there is a large variation in Λ when the temperatures are not the same. When $T_R < T_M$, the scale factor is larger than unity, and equation (44) shows that the steady-state ratio M_r/M_d is larger than the LTE ratio. This change of scale is important whenever radiative transitions are more probable than inelastic collisions. In such cases, the usual detailed balance assumption $\Lambda = 1$ cannot be used.

Figure 8 shows the steady-state rate constants for quadrupole association and dissociation of hydrogen. The M_r curves displayed in the top panel are reminiscent of the RA rate constants for H and D calculated by Stancil and Dalgarno [21] which included stimulated plus spontaneous radiative dipole transitions. In the present case, the rate constants for H_2 formation are about 100 times smaller than for HD formation. The modification in the rate constants due to the non-LTE concentration defects δ_u is seen to be significant, however, the net effect is still very small due to the weak radiative coupling. The bottom panel of Figure 8 shows the dissociation rate constant M_d as a function of T_R . There is no dependence on T_M at the level of resolution of the plot. Also shown are rate constants for photoionization



and indirect photodissociation



which occurs via dipole transitions to the Lyman and Werner systems. Both of these rate constants are taken from the fitting formulas given in Coppola et al. [22]. The photodissociation rate constant for quadrupole radiation dominates the other H_2 photodestruction rate constants for $T_R \leq 3000$ K. For a more general radiation field comprised of low energy photons, the quadrupole transitions would likewise provide the strongest mechanism for photodestruction of H_2 . Because the first luminous sources produced diluted blackbody fields with $T_R > 10,000$ K, the quadrupole mechanism is not expected to make a significant contribution to the suppression of H_2 molecules.

4. Discussion

With the rate constants described above, we may assess the significance of quadrupole association and dissociation on the formation of H_2 in the early universe. The rate constants shown in Figure 8 are extremely small and would be unimportant in all but the most extreme environments. The H^- sequence



is known to be the dominant H_2 formation mechanism in the early universe when the radiation field was weak [4, 5]. For redshift $z > 100$, the cosmic background radiation destroys H^- through the reverse of process (47). In this case, the RA processes



followed by



are the dominant H_2 formation mechanisms. These mechanisms are also destroyed by the cosmic background radiation at high redshifts through the reverse of processes (49) and (50). Because the binding energies of H_2^+ and HeH^+ are smaller than the binding energy of H_2 , they are more easily photodissociated than H_2 , and the quadrupole mechanisms may be significant. To see whether this is indeed the case, we substitute M_r and M_d into the rate equation (2) and assume that no other processes contribute. The steady-state solution is

$$[H_2]_{ss} = \left(\frac{n_H}{2}\right)^2 (\alpha + \beta)^{-1} . \quad (53)$$

Figure 9 shows the steady-state fractional population of H_2 versus n_H for several values of T_R . As n_H gets large, the ratio increases towards a limiting value of $1/2$ indicating that the gas has become completely molecular. This is not a realistic limit, however, because the time needed to reach the steady-state for quadrupole association is extremely long. The bottom panel of Figure 9 shows the time to reach one-half of the steady-state concentration

$$t_{1/2} = \lambda^{-1} \ln \left(\frac{3\alpha + \beta}{\alpha + \beta} \right) . \quad (54)$$

This time scale is larger than the age of the universe for low temperatures and densities. At the higher temperatures needed to reach steady-state on a more realistic time scale, the fractional population of H_2 drops substantially due to the increased efficiency of photodissociation. The bottom panel of Figure 9 shows that steady-state is obtainable within 10^5 years for $T_R \geq 2500$ K which corresponds to $n_H \approx 10^3 \text{ cm}^{-3}$. Using these numbers in the top panel shows that the fractional population of H_2 is of order 10^{-12} . For comparison, the formation mechanisms (49)-(52) yield a fractional population of H_2 which is between $10^{-11} - 10^{-15}$ when $500 < z < 1300$ [22]. The quadrupole mechanism cannot reach its steady-state limit for $T_R < 2500$ K, so it is necessary to use the time-dependent solution (4) to estimate the population. The dashed curve in the top panel of Figure 9 shows this solution for $z = 500 - 1300$ using the usual redshift formulas

$$t = (14 \times 10^9 \text{ yr})(1+z)^{-3/2} \quad (55)$$

$$T_R = (2.73 \text{ K})(1+z) \quad (56)$$

$$n_H = (10^{-6} \text{ cm}^{-3})(1+z)^3 . \quad (57)$$

All calculations used $M_r = 10^{-28} \text{ cm}^3/\text{s}$ so there is no T_M -dependence in the plots. Figure 8 shows this should be a good approximation for the values of T_R considered. The fractional population is found to have a maximum near $z = 800$ and a value of 10^{-13} at $z = 1000$. The maximum represents the optimal balance between the density and time needed to recombine and the destructive efficiency of photodissociation. The results for this restricted model demonstrate that the quadrupole mechanism is competitive with the standard formation mechanisms (49)-(52) for these high redshifts and perhaps even dominates for $800 < z < 1300$.

5. Conclusions

A theoretical formalism is described for H_2 which allows radiative association and photodissociation rate constants to be computed self-consistently for quadrupole transitions. The impact of extremely long-lived resonances is considered for LTE and non-LTE conditions that were prevalent in the early universe. Simple formulas are presented which may be used to compute the non-LTE concentration defects for any combination of matter and radiation temperature. It is found that the bound state defects δ_b at temperature T_M yield a good approximation to a Boltzmann equilibrium distribution at temperature T_R in the limiting case where inelastic collisions and charge transfer reactions are negligible. The unbound defects δ_u for the quasibound states were found to be quite large for $T_M \ll T_R$ and $T_M \gg T_R$, but do not substantially increase the formation rate constant due to the large exponential decay in the Boltzmann factor at small T_M and the increasing value of Q_T at large T_M . The photodissociation rate constant for quadrupole transitions is found to dominate the rate constants for other H_2 photodestruction mechanisms for $T_R \leq 3000$ K. It is demonstrated that quadrupole association and dissociation of hydrogen is generally inefficient but may have occurred in the early universe for $z > 500$.

Acknowledgments

The author acknowledges support from NSF Grant No. PHY-1503615.

References

- [1] Saslaw W C, and Zipoy D 1967 *Nature* **216** 976
- [2] Peebles P J E, and Dicke R H 1968 *Astrophysical Journal* **154** 891
- [3] Palla F, Salpeter E E, and Stahler S W 1983 *Astrophysical Journal* **271** 632
- [4] Lepp S, Stancil P C, and Dalgarno A 2002 *J. Phys. B: At. Mol. Phys.* **35** R57–R80
- [5] Kreckel H, Bruhns H, Cizek M, Glover S C O, Miller K A, Urbain X, and Savin D W 2010 *Science* **329** 69
- [6] Turner J, Kirby-Docken K, and Dalgarno A 1977 *Astrophys. J. Supp.* **35** 281
- [7] Wolniewicz L, Simbotin I, and Dalgarno A 1998 *Astrophys. J. Supp.* **115** 293
- [8] Forrey R C 2015 *J. Chem. Phys.* **143** 024101 URL <http://dx.doi.org/10.1053/1.4926325/>
- [9] Forrey R C, Babb J F, Stancil P C, and McLaughlin B M submitted *J. Phys. B*
- [10] Schwenke D W 1988 *Theor. Chim. Acta* **381**
- [11] Bromm V, and Loeb A 2003 *Astrophysical Journal* **596** 34
- [12] Sugimura K, Omukai K, and Inoue A K 2014 *Mon. Not. Roy. Astr. Soc.* **445** 554
- [13] Sugimura K, Coppola C M, Omukai K, Galli D, and Palla F 2016 *Mon. Not. Roy. Astr. Soc.* **456** 270
- [14] Hummer D G, Rybicki G 1971 *Annual Reviews* 237
- [15] De Jong T, Chu S-I, and Dalgarno A 1975 *Astrophysical Journal* **199** 69
- [16] Bain R A and Bardsley J N 1972 *J. Phys. B: At. Mol. Phys.* **5** 277 URL <http://iopscience.iop.org/0022-3700/5/2/024/>
- [17] Forrey R C 2013 *Phys. Rev. A* **88** 052709 URL <http://dx.doi.org/10.1103/PhysRevA.88.052709/>
- [18] Bennett O J, Dickinson A S, Leininger T and Gad  a X 2003 *Mon. Not. Roy. Astr. Soc.* **341** 361 URL <http://dx.doi.org/10.1046/j.1365-8711.2003.06422.x/>
- [19] Gutafsson M, Antipov S V, Franz J and Nyman G 2012 *J. Chem. Phys.* **137** 104301 URL <http://dx.doi.org/10.1063/1.4750029/>
- [20] Antipov S V, Gustafsson M and Nyman G 2013 *Mon. Not. Roy. Astr. Soc.* **430** 946 URL <http://dx.doi.org/10.1093/mnras/sts615/>
- [21] Stancil P C, and Dalgarno A 1997 *Astrophysical Journal* **490** 76
- [22] Coppola C M, Longo S, Capitelli M, Palla F, Galli D 2011 *Astrophysical Journal Supplement Series* **193** 7

Table 1. Einstein A-coefficients (s^{-1}) for radiative transitions between quasibound and bound states of H_2 . The rotational level j of the quasibound state and vibrational level v of the bound state are arranged in columns. The coefficients for transitions to rotational levels $j - 2, j, j + 2$ are shown for each v .

v	$j = 4$	$j = 13$	$j = 15$	$j = 17$	$j = 19$	$j = 21$	$j = 23$
0	4.25(-13)	1.15(-10)	3.04(-10)	6.35(-10)	1.20(-9)	2.06(-9)	3.03(-9)
	1.12(-14)	3.92(-13)	1.94(-12)	7.17(-12)	2.45(-11)	8.20(-11)	2.83(-10)
	7.12(-13)	4.74(-12)	9.41(-12)	1.69(-11)	3.19(-11)	6.63(-11)	1.59(-10)
1	7.46(-12)	1.37(-9)	3.42(-9)	6.60(-9)	1.12(-8)	1.61(-8)	1.64(-8)
	2.44(-15)	1.19(-11)	4.79(-11)	1.55(-10)	4.80(-10)	1.51(-9)	5.13(-9)
	8.34(-12)	6.52(-11)	1.30(-10)	2.35(-10)	4.51(-10)	9.60(-10)	2.01(-9)
2	6.62(-11)	8.17(-9)	1.88(-8)	3.26(-8)	4.69(-8)	4.85(-8)	1.55(-8)
	7.42(-13)	1.53(-10)	5.37(-10)	1.58(-9)	4.62(-9)	1.43(-8)	4.33(-8)
	4.76(-11)	4.43(-10)	8.96(-10)	1.64(-9)	3.17(-9)	5.61(-9)	5.30(-9)
3	3.94(-10)	3.18(-8)	6.60(-8)	9.77(-8)	1.04(-7)	4.07(-8)	4.61(-8)
	1.82(-11)	1.18(-9)	3.77(-9)	1.05(-8)	3.01(-8)	8.05(-8)	1.42(-7)
	1.71(-10)	1.98(-9)	4.07(-9)	7.31(-9)	1.10(-8)	7.87(-9)	1.46(-10)
4	1.76(-9)	8.90(-8)	1.59(-7)	1.76(-7)	7.91(-8)	3.41(-8)	9.74(-7)
	1.72(-10)	6.42(-9)	1.97(-8)	5.31(-8)	1.26(-7)	1.86(-7)	8.13(-8)
	4.13(-10)	6.39(-9)	1.24(-8)	1.59(-8)	8.15(-9)	2.33(-11)	8.08(-10)
5	6.21(-9)	1.83(-7)	2.46(-7)	1.22(-7)	2.10(-8)	8.44(-7)	1.54(-6)
	1.00(-9)	2.80(-8)	8.09(-8)	1.72(-7)	2.14(-7)	7.43(-8)	5.43(-11)
	6.44(-10)	1.31(-8)	1.60(-8)	4.90(-9)	1.06(-9)	1.43(-9)	
6	1.80(-8)	2.49(-7)	1.50(-7)	1.15(-8)	6.72(-7)	1.08(-6)	1.34(-7)
	4.31(-9)	9.45(-8)	2.03(-7)	2.14(-7)	5.88(-8)	6.74(-13)	
	4.62(-10)	7.63(-9)	5.15(-10)	4.78(-9)	2.21(-9)		
7	4.46(-8)	1.28(-7)	6.53(-9)	4.89(-7)	6.85(-7)	6.71(-8)	
	1.53(-8)	1.78(-7)	1.80(-7)	3.87(-8)	6.69(-11)		
	6.13(-11)	2.07(-9)	1.17(-8)	2.88(-9)			
8	9.01(-8)	4.65(-9)	3.17(-7)	3.87(-7)	3.00(-8)		
	4.41(-8)	1.05(-7)	1.93(-8)	1.88(-10)			
	8.28(-9)	1.65(-8)	2.99(-9)				
9	1.15(-7)	1.56(-7)	1.83(-7)	1.14(-8)			
	7.86(-8)	5.30(-9)	2.64(-10)				
	4.40(-8)	1.97(-8)					
10	5.38(-8)	5.88(-8)	3.36(-9)				
	5.42(-8)	1.98(-10)					
	5.49(-8)						
11	1.70(-9)	5.78(-10)					
	6.54(-9)						
	1.26(-8)						
12	1.28(-9)						
	2.61(-11)						
	1.69(-10)						
13	1.07(-10)						
	9.82(-12)						
	1.07(-14)						
14	6.71(-15)						

Table 2. Same as Table 1 but for $j = 24 - 29$.

v	$j = 24$	$j = 25$	$j = 26$	$j = 27$	$j = 28$	$j = 29$	$j = 29$
0	4.46(-9)	3.06(-9)	1.79(-9)	3.55(-10)	8.65(-9)	2.24(-7)	1.95(-8)
	1.01(-9)	1.08(-9)	4.27(-9)	4.44(-9)	1.57(-8)	3.14(-8)	1.47(-8)
	4.36(-10)	4.02(-10)	8.13(-10)	6.45(-10)	2.92(-10)	2.70(-11)	1.46(-10)
1	1.14(-8)	3.74(-9)	1.45(-8)	4.06(-8)	5.79(-7)	2.95(-6)	7.28(-7)
	1.76(-8)	1.79(-8)	5.14(-8)	4.67(-8)	5.95(-8)	5.15(-9)	4.32(-8)
	3.23(-9)	2.47(-9)	7.48(-10)	3.37(-10)	9.79(-11)		
2	1.25(-8)	5.00(-8)	7.52(-7)	9.51(-7)	3.05(-6)	1.87(-6)	2.89(-6)
	1.04(-7)	9.17(-8)	9.21(-8)	6.44(-8)	2.46(-9)		
	9.83(-10)	3.67(-10)	3.05(-10)				
3	8.02(-7)	1.02(-6)	2.75(-6)	2.54(-6)	9.87(-7)	2.58(-10)	7.48(-7)
	1.16(-7)	7.79(-8)	1.92(-9)	5.26(-10)			
	7.57(-10)	3.97(-10)					
4	2.27(-6)	2.05(-6)	6.01(-7)	4.40(-7)			
	1.24(-9)	2.41(-10)					
5	3.53(-7)	2.49(-7)					
6	1.65(-11)						

Table 3. Same as Table 1 but for $j = 30 - 33$.

v	$j = 30$	$j = 31$	$j = 31$	$j = 32$	$j = 32$	$j = 33$	$j = 33$
0	2.93(-7)	2.10(-6)	3.69(-7)	4.73(-6)	2.15(-6)	4.34(-6)	2.14(-6)
	2.52(-8)	3.60(-9)	1.90(-8)				
1	2.97(-6)	2.87(-6)	2.88(-6)	3.60(-10)	2.49(-6)		
	2.59(-9)						
2	1.58(-6)						

Table 4. Einstein A-coefficients (s^{-1}) for radiative transitions between quasibound states of H_2 . For rotational levels with more than one quasibound state, the entries are listed according to $j_{u_f} = j_{u_i} - 2$ starting with the lowest E_{u_i} and E_{u_f} , and ending with the $j_{u_f} = j_{u_i}$ transition.

j_{u_i}	$A_{u_i \rightarrow u_f}$	j_{u_i}	$A_{u_i \rightarrow u_f}$	j_{u_i}	$A_{u_i \rightarrow u_f}$	j_{u_i}	$A_{u_i \rightarrow u_f}$	j_{u_i}	$A_{u_i \rightarrow u_f}$
15	1.29(-20)	26	7.43(-11)	30	5.08(-10)	32	1.88(-11)	33	1.47(-9)
17	4.50(-16)	27	1.83(-10)	31	4.96(-10)	32	8.74(-10)	33	8.56(-10)
19	8.10(-14)	28	2.25(-10)	31	5.17(-11)	32	1.94(-9)	34	3.88(-6)
21	1.60(-12)	29	1.55(-10)	31	1.24(-6)	33	6.14(-10)	34	1.01(-9)
23	1.24(-11)	29	4.56(-10)	31	9.19(-10)	33	1.11(-11)	35	3.34(-6)
25	5.66(-11)	29	8.26(-10)	31	1.01(-9)	33	2.04(-6)	35	1.64(-9)

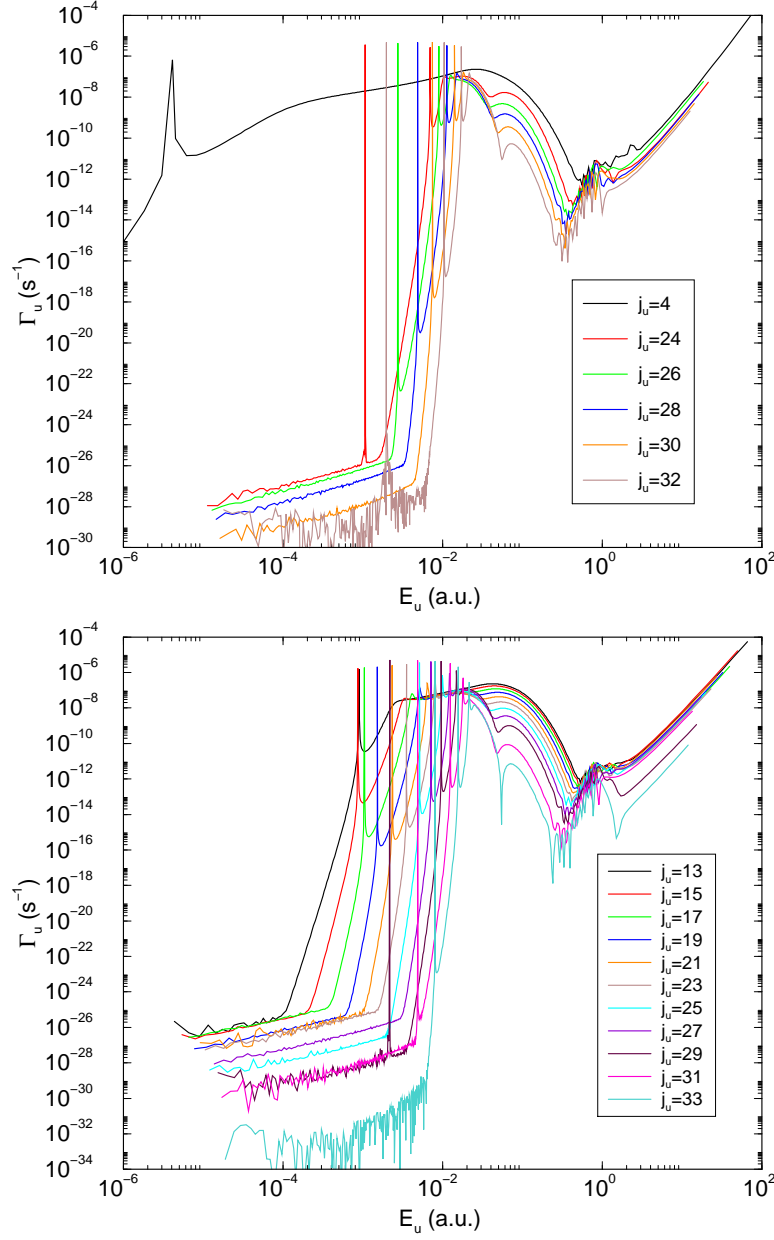


Figure 1. Radiative association width (42) for the formation of para-H₂ (top) and ortho-H₂ (bottom). Partial waves that support long-lived quasibound states are shown. The resonance peaks correspond to summed columns in Tables 1-3.

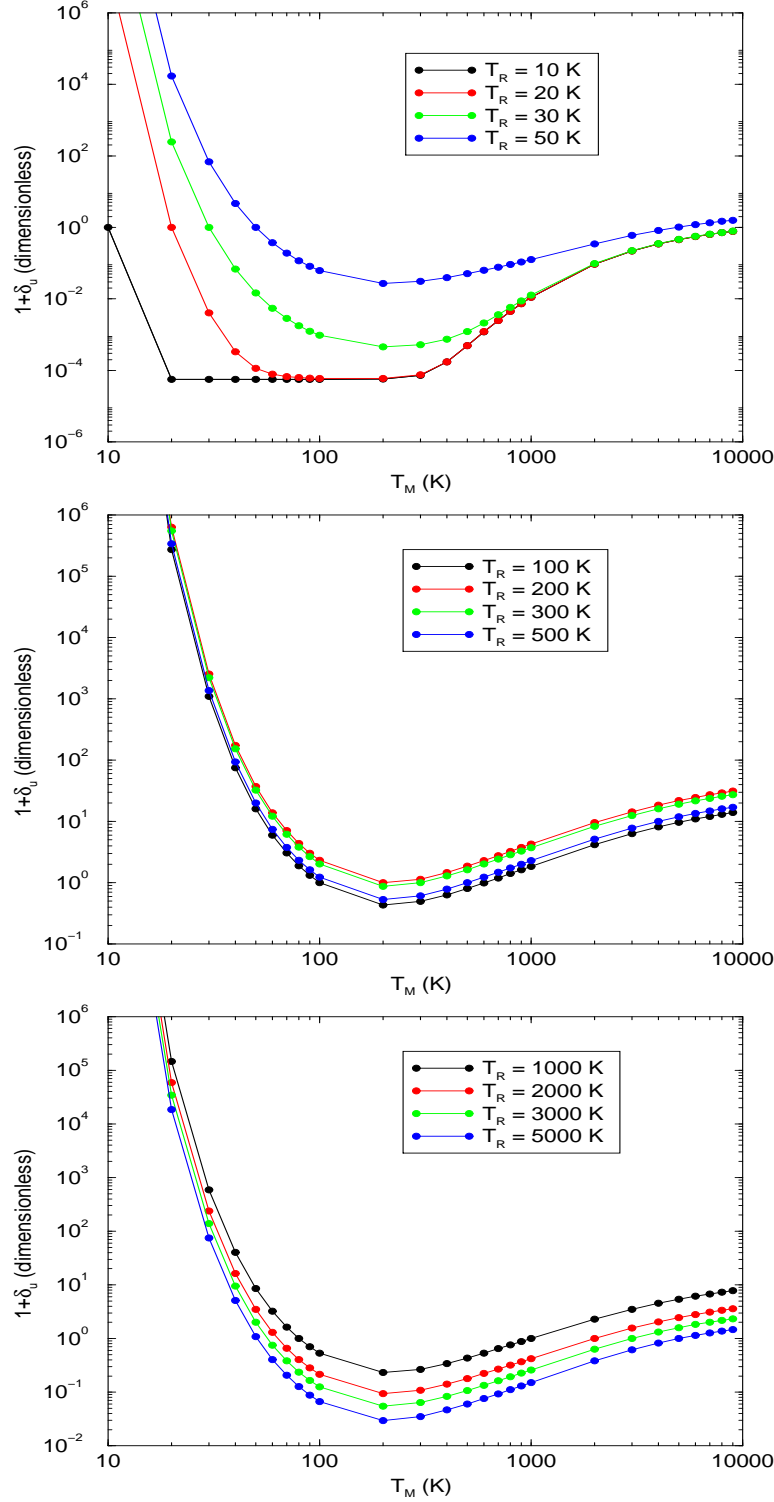


Figure 2. Non-LTE concentration factor for the $j=24$ quasibound state of H_2 . Low values of T_R tend to deplete the resonant state for $T_M > T_R$. Intermediate values of T_R tend to increase the quasibound concentration beyond the LTE value, especially at low T_M . Large values of T_R tend to deplete the quasibound state at intermediate T_M while enhancing the concentration at low and high T_M .

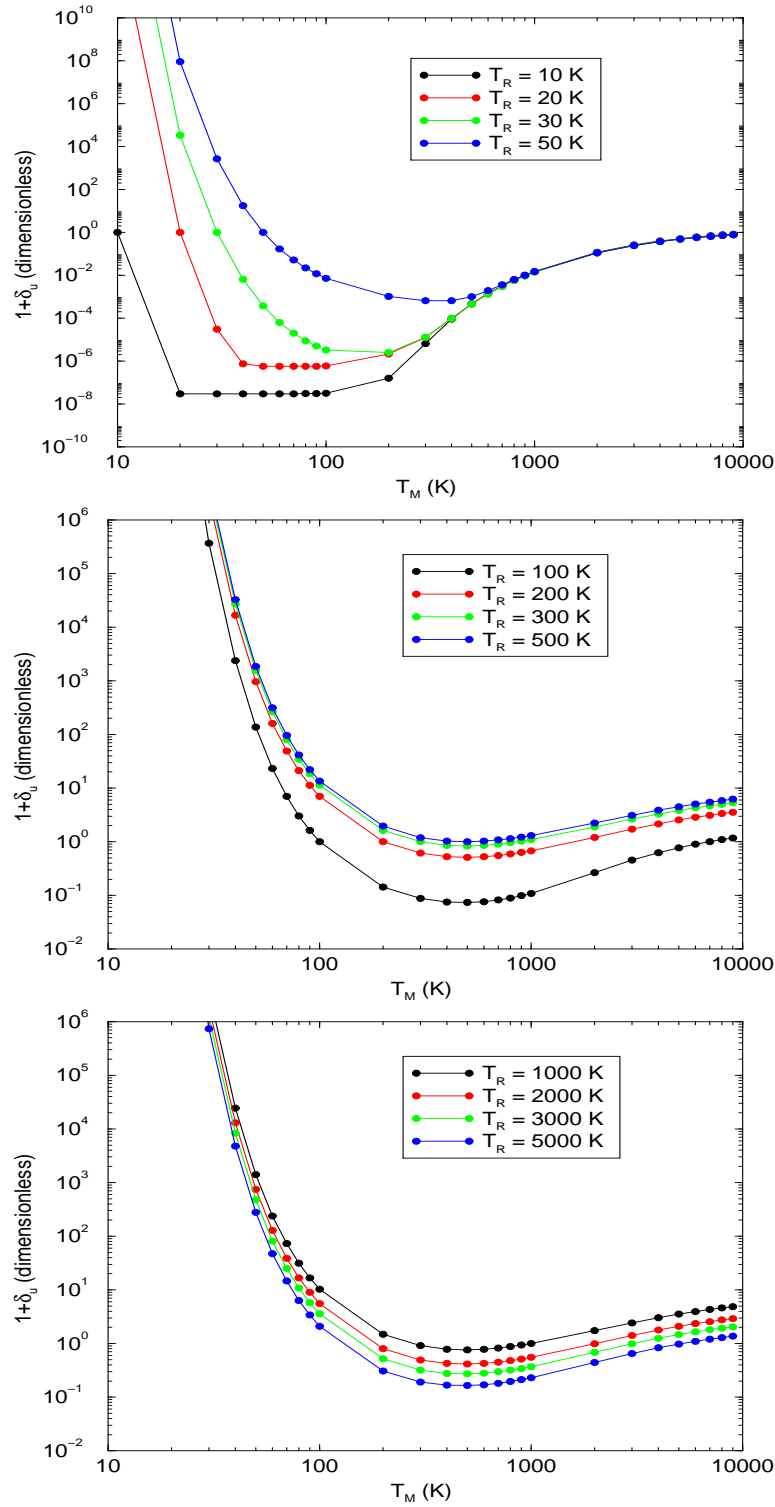


Figure 3. Same as Figure 2 except for $j=29$.

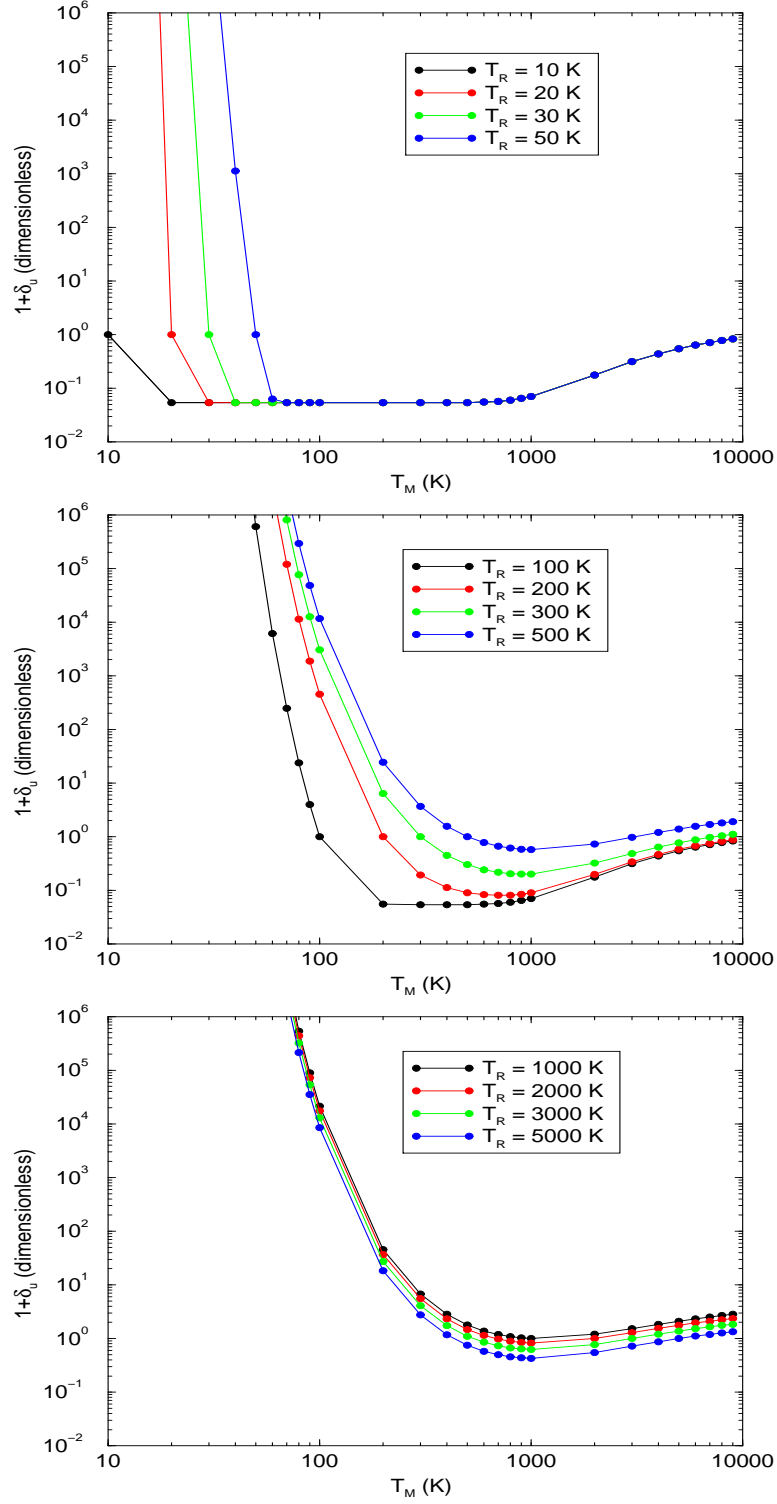
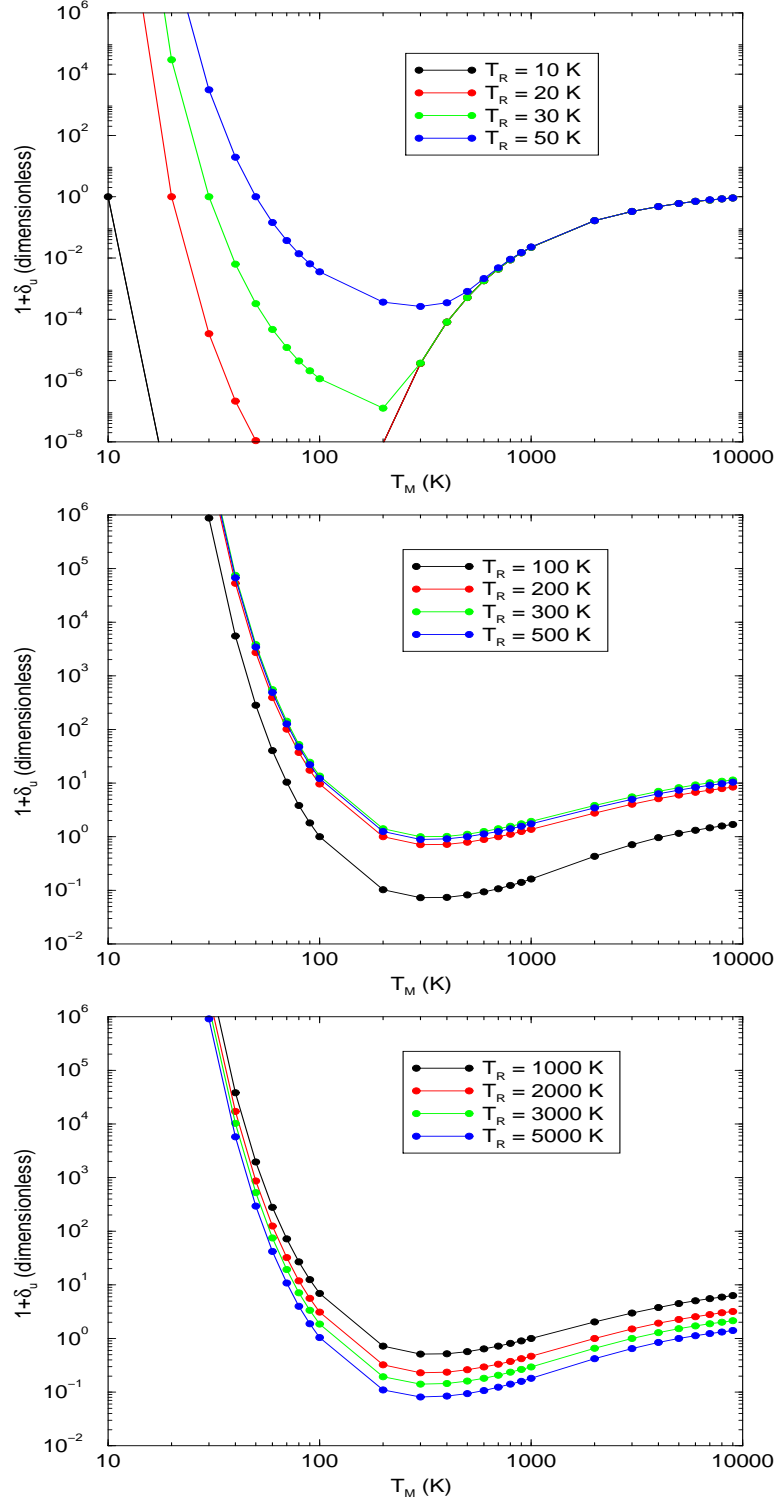


Figure 4. Same as Figure 2 except for $j=31$.


 Figure 5. Same as Figure 2 except for $j=32$.

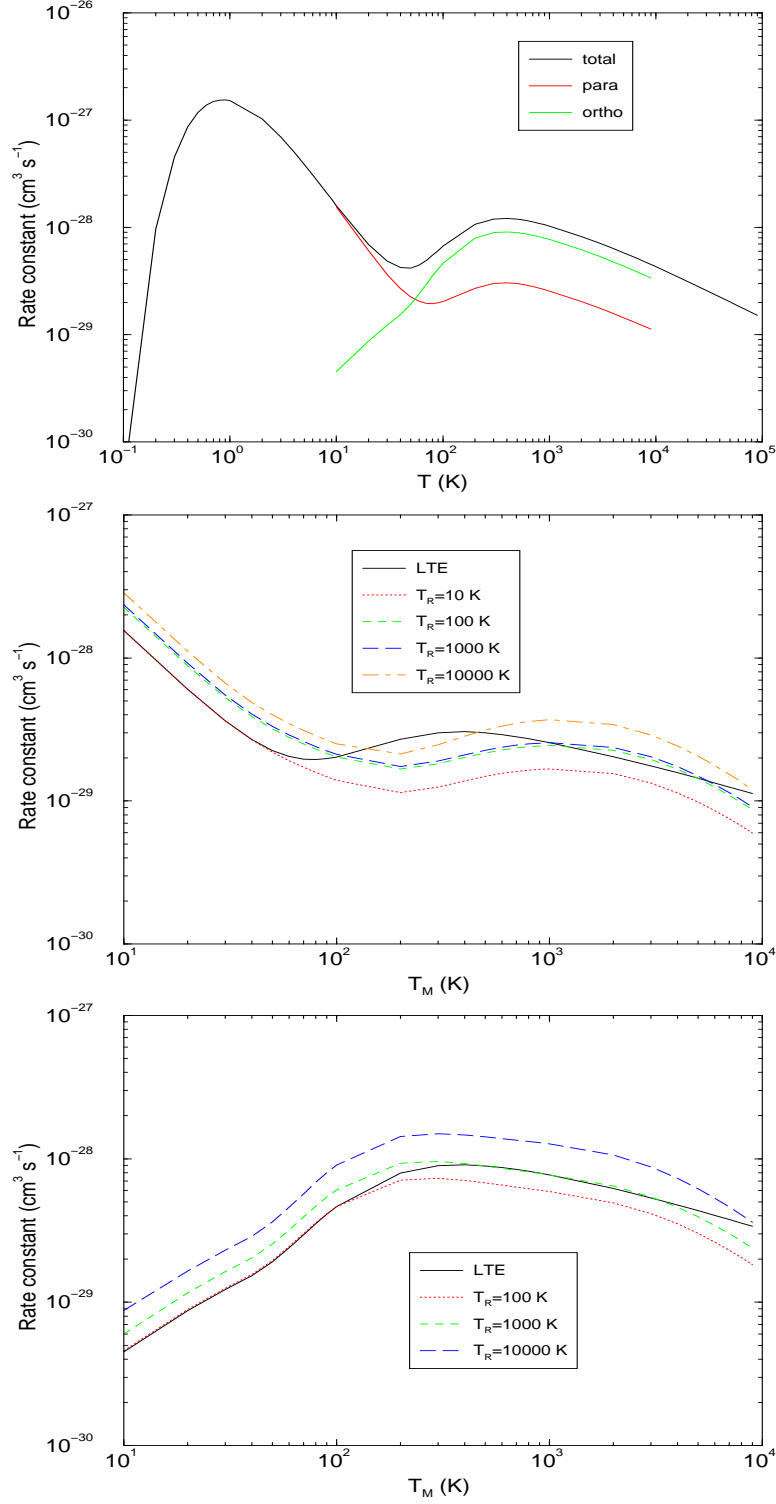


Figure 6. Rate constant for radiative association of H_2 at LTE (top panel). Also shown are non-LTE rate constants as a function of T_R and T_M for forming para- H_2 (middle panel) and ortho- H_2 (bottom panel).

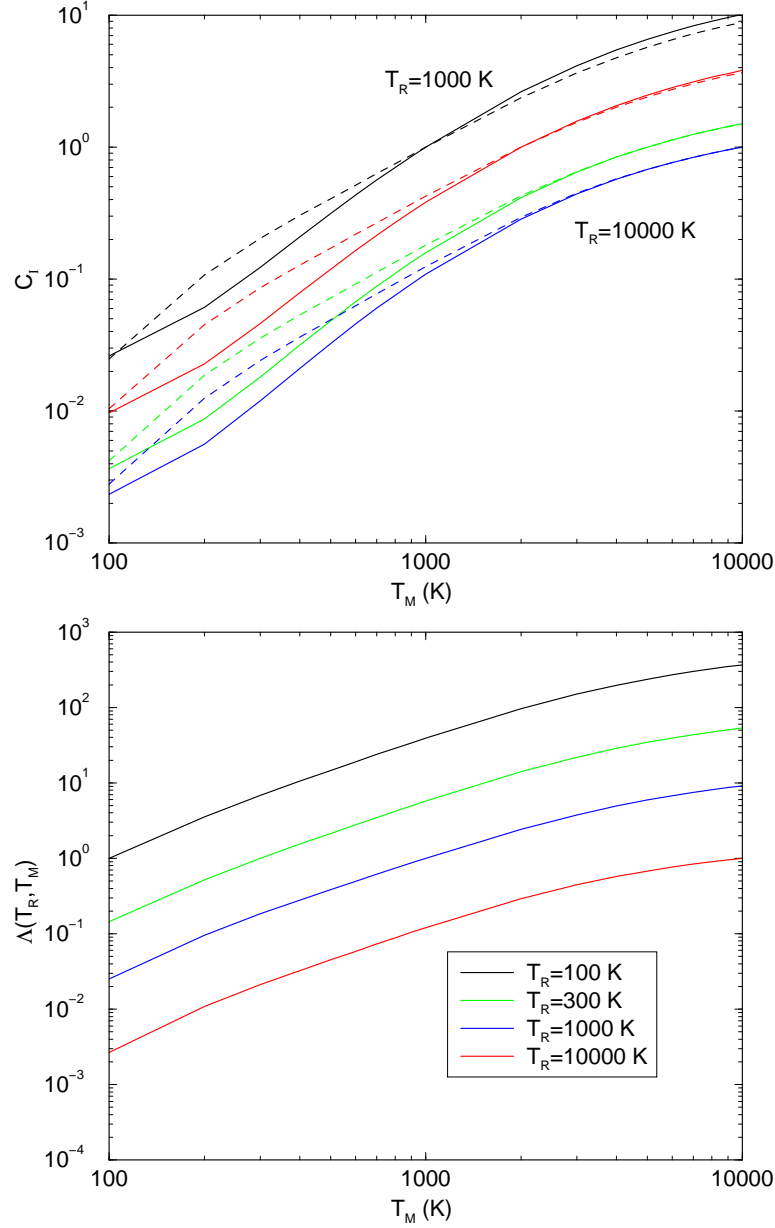


Figure 7. Symmetry constants C_I (top panel) and scale factor Λ (bottom panel). The symmetry constants are plotted for $T_R = 1000, 2000, 5000$, and 10000 K using solid lines for $I = 0$ and dashed lines for $I = 1$. The scale factor is unity for $T_R = T_M$ but otherwise shows strong variation due to the assumed absence of inelastic three-body collisions.

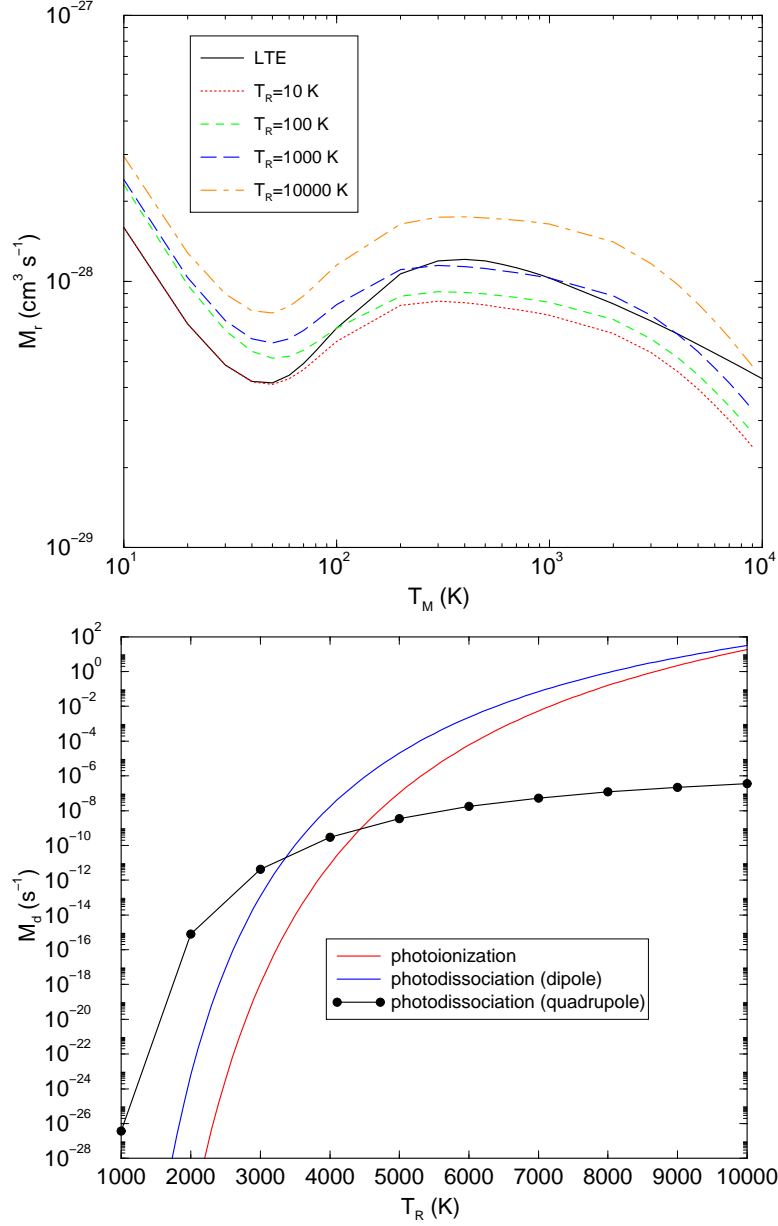


Figure 8. Steady-state rate constants M_r (top panel) and M_d (bottom panel). The dissociation rate constant has a very weak dependence on T_M and is plotted as a function of T_R . Also shown on the bottom panel are rate constants for photoionization and indirect photodissociation (dipole) obtained from [22].

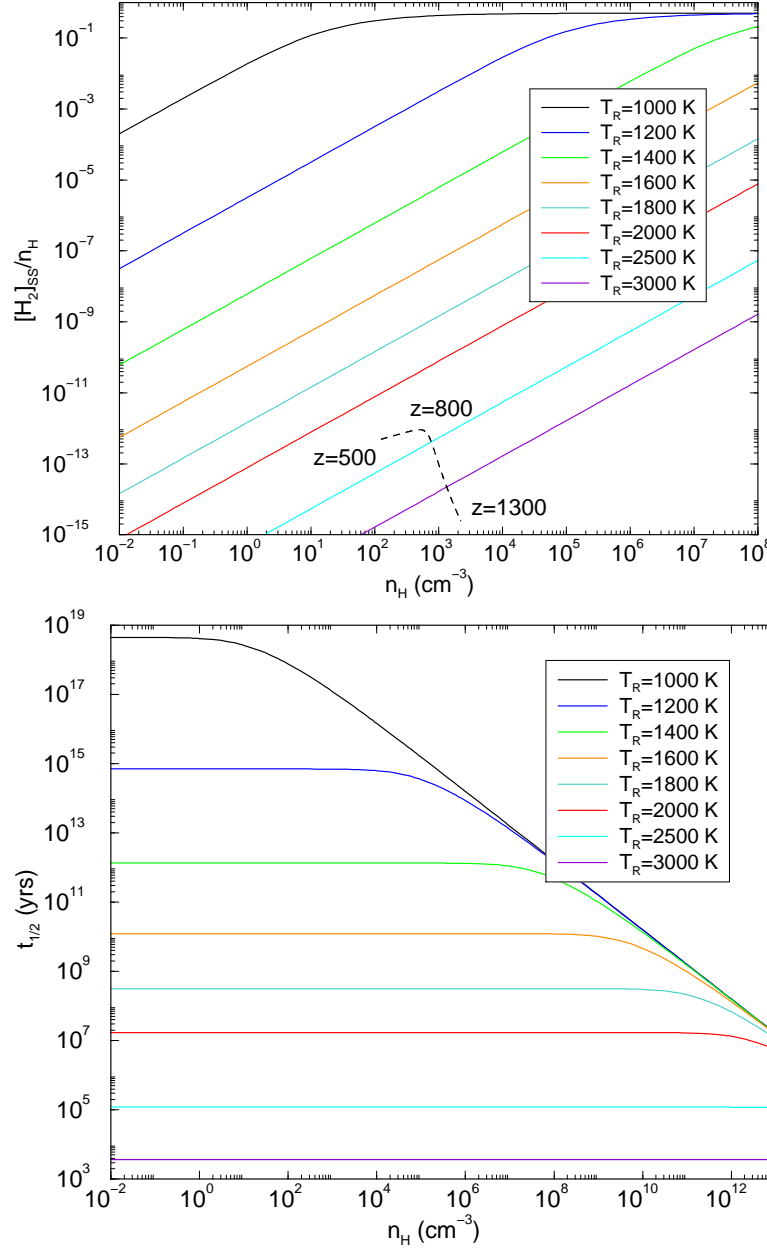


Figure 9. Steady-state fractional population of H_2 (top panel) and the time required to reach one-half the steady-state value (bottom panel) for a system which considers only quadrupole association and dissociation of hydrogen. When $T_{\text{R}} < 2500$ K, the system is not able to reach steady-state on a realistic time scale. In this case, the time-dependent solution (4) is shown as a dashed curve on the top panel for $500 < z < 1300$.